International Journal of Heat and Mass Transfer

Droplet Evaporation on Hot Micro-structured Superhydrophobic Surfaces: Analysis of Evaporation from Droplet Cap and Base Surfaces
--Manuscript Draft--

Manuscript Number:	
Article Type:	Full Length Article
Keywords:	droplet evaporation; micro-structured surfaces; superhydrophobic surfaces; thermal circuit analysis; depressed boiling
Corresponding Author:	Jiangtao Cheng Virginia Polytechnic Institute and State University Blacksburg, VA UNITED STATES
First Author:	Wenge Huang
Order of Authors:	Wenge Huang
	Xukun He, PhD
	Cong Liu
	Xiaojie Li
	Yahua Liu
	Jiangtao Cheng
Abstract:	In this study, evaporation of sessile water droplets on hot micro-structured superhydrophobic surfaces is experimentally and theoretically investigated. Water droplets of 4 µL are placed on micro-pillared silicon substrates with the substrate temperature heated up to 120 °C. A comprehensive thermal circuit model is developed to analyze the effects of substrate roughness and substrate temperature on the sessile droplet evaporation. For the first time, two components of heat and mass transfer, i.e ., one from the droplet cap surface and the other from the droplet base surface, during droplet evaporation are distinguished and systematically studied. As such, the evaporation rates from both the droplet cap surface and the interstitial liquid-vapor interface between micropillars at the droplet base are calculated in various conditions. For droplet evaporation on the heated substrates in the range of 40 °C – 80 °C, the predicted droplet cap temperature matches well with the experimental results. During the constant contact radius mode of droplet evaporation, the decrease of evaporation rate from the droplet base contributes most to the continuously decreasing total evaporation rate, whereas the decrease of evaporation rate from the droplet cap surface is dominant in the constant contact angle mode. The influence of internal fluid flow is considered for droplet evaporation on substrates heated above 100 °C, and an effective thermal conductivity is adopted as a correction factor to account for the effect of convection heat transfer inside the droplet. Temperature differences between the droplet base and the substrate surface are estimated to be ~ 2 °C, 5 °C, 8 °C, 12.5 °C and 18 °C for droplet evaporation on substrates heated at 40 °C, 60 °C, 80 °C, 100 °C, and 120 °C, respectively, which can elucidate the delayed or depressed boiling of water droplets on a heated rough surface.
Suggested Reviewers:	Zuankai Wang, PhD Professor, City University of Hong Kong zuanwang@cityu.edu.hk Well-known scholar in wetting and heat transfer
	Nenad Miljkovic, PhD Associate Professor, University of Illinois at Urbana-Champaign nmiljkov@illinois.edu Well-known professor in heat transfer
	Arun Kumar Kota, PhD Assistant Professor, North Carolina State University Department of Mechanical and Aerospace Engineering akota2@ncsu.edu

	Expert in wetting and heat transfer
	Chuanhua Chen, PhD Associate Professor, Duke University chuanhua.chen@duke.edu Famous professor in heat transfer
	Charles Patrick Collier, PhD Staff Researcher, Oak Ridge National Laboratory colliercp@ornl.gov Established scientist in nano-engineering and heat transfer
Opposed Reviewers:	

Dear Editor,

We are pleased to submit our manuscript entitled "Droplet Evaporation on Hot Micro-structured Superhydrophobic Surfaces: Analysis of Evaporation from Droplet Cap and Base Surfaces" to *International Journal of Heat and Mass Transfer* for consideration as an original research article. In this study, sessile droplet evaporation on hot micro-structured superhydrophobic surfaces is experimentally and theoretically investigated. For the first time, two components of heat and mass transfer, *i.e.*, one from the droplet cap surface and the other from the droplet base surface, during droplet evaporation are distinguished and systematically studied. We believe that this manuscript is appropriate for publication in *International Journal of Heat and Mass Transfer*. The traits of this work are:

- We conducted a comprehensive thermal resistance analysis about the sessile droplet evaporation on hot micro-structured superhydrophobic substrates by analyzing evaporation from both the droplet cap surface and the droplet base surface. It is found that droplet cap surface temperature shows distinct trends in different evaporation modes, *i.e.*, droplet cap surface temperature increases in the constant contact radius (CCR) mode while keeping almost constant in the constant contact angle (CCA) mode.

- Evaporation rates from both the droplet cap and the droplet base are calculated in various conditions. During the CCR mode of droplet evaporation, the decrease of evaporation rate from the droplet base contributes most to the continuously decreasing total evaporation rate, whereas the decrease of evaporation rate from the droplet cap surface is dominant in the CCA mode.

- The ratio φ of droplet base evaporation rate to the total evaporation rate decreases in the CCR mode and increases approaching the end of the CCA mode. For droplets with a relatively large volume, φ increases with the rise of the substrate temperature; and for droplets with a small volume, φ decreases with the rise of the substrate temperature.

- Temperature differences between the droplet base and the substrate surface are estimated to be ~ 2 °C, 5 °C, 8 °C, 12.5 °C and 18 °C for droplet evaporation on substrates heated at 40 °C, 60 °C, 80 °C, 100 °C, and 120 °C, respectively, which can elucidate the delayed or depressed boiling of water droplets on a heated rough surface.

All authors listed in the paper have contributed to this work. To the best of our knowledge, no conflicts of interest, financial or others exist. We have included acknowledgements and financial information in the manuscript. PDF of manuscript is in correct order upon submission.
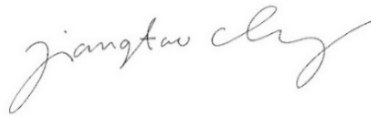
This manuscript has not been previously published and is not under consideration in the same or substantially similar form in any other peer review media. All data needed to evaluate the conclusions in the paper are present in the paper and the Supplementary Materials. The prepared manuscript is in compliance with the Ethics in publishing as described in Author Guidelines.

In addition, we suggest the following five reviewers for our submission:

1. Zuankai Wang, PhD
   Professor, City University of Hong Kong
   Email: zuanwang@cityu.edu.hk

2. Nenad Miljkovic, PhD
   Associate Professor, University of Illinois at Urbana-Champaign
   Email: nmiljkov@illinois.edu

3. Arun Kumar Kota, PhD
   Assistant Professor, North Carolina State University
   Email: akota2@ncsu.edu

4. Chuanhua Chen, PhD
   Associate Professor, Duke University
   Email: chuanhua.chen@duke.edu

5. Charles Patrick Collier, PhD
   Staff Researcher, Oak Ridge National Laboratory
   Email: colliercp@ornl.gov
   https://www.ornl.gov/staff-profile/pat-p-collier

Yours Sincerely,

Jiangtao Cheng
Associate Professor
Department of Mechanical Engineering
Virginia Polytechnic Institute and State University
Email: chengjt@vt.edu, Phone: (+1) 540-231-4164

Droplet Evaporation on Hot Micro-structured Superhydrophobic Surfaces: Analysis of Evaporation from Droplet Cap and Base Surfaces

Wenge Huang [a †], Xukun He [a †], Cong Liu [d], Xiaojie Li [d], Yahua Liu [d], Jiangtao Cheng [a, b, c, *]

[a] Department of Mechanical Engineering, Virginia Tech, Blacksburg, VA 24061, USA

[b] Macromolecules Innovation Institute, Virginia Tech, Blacksburg, VA 24061, USA

[c] Center for Soft Matter and Biological Physics, Virginia Tech, Blacksburg, VA 24061, USA

[d] Key Laboratory for Non-traditional Machining Technology of Ministry of Education, Dalian University of Technology, Dalian 116024, China

*Corresponding author. E-mail: chengjt@vt.edu; Phone: 540-231-4164

Abstract: In this study, evaporation of sessile water droplets on hot micro-structured superhydrophobic surfaces is experimentally and theoretically investigated. Water droplets of 4 µL are placed on micro-pillared silicon substrates with the substrate temperature heated up to 120 °C. A comprehensive thermal circuit model is developed to analyze the effects of substrate roughness and substrate temperature on the sessile droplet evaporation. For the first time, two components of heat and mass transfer, *i.e.*, one from the droplet cap surface and the other from the droplet base surface, during droplet evaporation are distinguished and systematically studied. As such, the evaporation rates from both the droplet cap surface and the interstitial liquid-vapor interface between micropillars at the droplet base are calculated in various conditions. For droplet evaporation on the heated substrates in the range of 40 °C – 80 °C, the predicted droplet cap temperature matches well with the experimental results. During the constant contact radius mode of droplet evaporation, the decrease of evaporation rate from the droplet base contributes most to the continuously decreasing total evaporation rate, whereas the decrease of evaporation rate from the droplet cap surface is dominant in the constant contact angle mode. The influence of internal fluid flow is considered for droplet evaporation on substrates heated above 100 °C, and an effective thermal conductivity is adopted as a correction factor to account for the effect of convection heat transfer inside the droplet. Temperature differences between the droplet base and the substrate surface are estimated to be ~ 2 °C, 5 °C, 8 °C, 12.5 °C and 18 °C for droplet evaporation on substrates heated at 40 °C, 60 °C, 80 °C, 100 °C, and 120 °C, respectively, which can elucidate the delayed or depressed boiling of water droplets on a heated rough surface.

Keywords: droplet evaporation, micro-structured surfaces, superhydrophobic surfaces, thermal circuit analysis, depressed boiling.

1. Introduction

Evaporation of sessile liquid droplets is a ubiquitous phenomenon in nature, which holds an important role in a variety of applications, including inkjet printing[1, 2], DNA mapping[3], spray cooling[4], analyte enrichment/detection[5], and colloidal assembly[2, 6]. Meanwhile, sessile droplet evaporation is a complex process controlled by several interdependent factors, such as droplet contact angle dynamics[7], contact line motion[6, 8-10], substrate structures[11-16] and temperature[17-22], and the surrounding environment[23-25].

Since the seminal work of Picknett and Bexon in 1977[26], sessile droplet evaporation on smooth surfaces has been systematically studied, in which droplet evaporation was distinguished into three evaporation modes: (1) constant contact radius (CCR) mode: the droplet contact line is pinned with a constant contact radius while the contact angle keeps decreasing; (2) constant contact angle (CCA) mode: once the contact angle approaches the receding contact angle, the contact line keeps receding with the contact angle unchanged; (3) mixed mode: both the contact radius and contact angle decrease near the end of evaporation. In several recent studies about the droplet evaporation on structured superhydrophobic surfaces, a special stick-slip mode[27] was observed, in which droplet contact line is moved by the pinning and depinning forces alternately.

Several theoretical models have been proposed to predict the evaporation rate of sessile droplets on various surfaces. In the classical work of Picknett and Bexon[26], the sessile droplet evaporation at room temperature was firstly assumed to be driven by vapor diffusion, ignoring the heat transfer and convective flow inside/outside the droplet. And the analytic evaporation rate could be obtained based on an analogy between the concentration field and the electrostatic field[28]. During the past two decades, this diffusion-driven model was extensively studied, which has been applied in modeling the evaporation of sessile droplets with an arbitrary contact angle in the CCR mode or with a slipping contact line in the CCA mode. The excellent agreement between the analytical evaporation rate and the experimental data confirms the validity of the diffusion-

driven model of sessile droplet evaporation not only on hydrophilic surfaces[29-31] but also on hydrophobic surfaces[22, 32].

However, when the diffusion-driven model was employed for analyzing sessile droplet evaporation on non-wetting surfaces with microstructures[33], especially on the heated superhydrophobic surfaces, an overestimation of evaporation rate was observed by Garimalla and Aldhaleai[34-36]. This deviation from the analytically predicted evaporation rate should result from evaporative cooling, giving rise to a temperature reduction on the liquid-vapor interface, which is in contradiction to the pivotal assumption in the classical diffusion-driven model that the temperature of the droplet surface is constant and same as the substrate temperature[29-31]. For instance, the maximum temperature mismatch of ~20 °C between the droplet surface and the substrate was experimentally observed when the substrate was heated at 70 °C[17]. Furthermore, the applicability of the diffusion-driven model might become worse when the wetting states of droplet on micro-structured surfaces, *i.e.*, the Cassie state or the Wenzel state[37], are considered. For the evaporation of a sessile droplet in the Cassie state, the existence of the air/vapor cushion layer between the droplet base and the microstructures would lead to two different components of droplet evaporation, *i.e.*, one from the liquid-vapor interface at the droplet cap and the other from the droplet base. However, the effect of this extra evaporative interface from the droplet base on superhydrophobic surfaces was generally ignored in the majority of previous word[34, 36, 38]. Indeed, in recent work of Wang and Kim[18, 39, 40], the non-negligible evaporation flux through the vapor-liquid interface over the substrate cavities has been experimentally confirmed on heated superhydrophobic surfaces, whereas these works mainly focused on the wetting or dynamics of the evaporating droplet. Therefore, a systematic study about droplet evaporation on heated micro-structured surfaces by considering the comprehensive effects of the multiple and discontinuous liquid-vapor interfaces at the droplet base and the continuous liquid-vapor interface at the droplet cap is entailed.

In this paper, the evaporation of water droplets on hot micro-structured superhydrophobic substrates is experimentally and theoretically investigated. Water droplets of 4 µL were placed on

the superhydrophobic substrates heated at 40 °C, 60, and 80 °C, respectively. The droplet evaporated in the Cassie state during the majority of its evaporation time and transited to the Wenzel state at the very end of evaporation. Based on a comprehensive thermal resistance analysis, a thermal circuit model was developed to predict the droplet cap surface temperature and to calculate the evaporation rates from the droplet cap surface and the base surface, respectively. An evaporation ratio φ, which is defined as the ratio of evaporation rate from the droplet base surface to the total evaporation rate, is analyzed in both the CCR mode and the CCA mode. And we found that the droplet surface temperature predicted by the thermal circuit model matches well with the experimental results. Both the evaporation rates from the droplet cap surface and the base surface decrease during droplet evaporation. The decrease of the evaporation rate from the droplet base surface contributes more to the decrease of the total evaporation rate in the CCR mode, whereas the decrease of evaporation rate from the droplet cap surface is dominant in the CCA mode. The evaporation ratio φ decreases in the CCR mode and increases approaching the end of the CCA mode. Then the substrate was further heated from 80 °C to 120 °C until a further small increase of the substrate temperature would otherwise lead to the boiling of the droplet. A remarkable deviation between the experimentally measured droplet surface temperature and the one predicted by thermal circuit analysis was observed for droplet evaporation at such a high substrate temperature, being that the internal fluid convection *i.e*., Marangoni effect[41], of the water droplet starts playing a more important role. As such, an effective thermal conductivity was adopted by us as a correction factor to account for the effect of convection heat transfer inside the water droplet. The average temperatures of the droplet base surface were calculated and the temperature differences between the droplet base and the substrate base were about 12.5 °C and 18 °C, respectively, for droplet evaporation on substrates heated at 100 °C and 120 °C, which explains the depressed or delayed boiling of droplets on the superheated substrates. This study could deepen our understanding of droplet evaporation on hot micro-structured surfaces and provide us a potential way to control the sessile droplet evaporation on non-wetting surfaces.
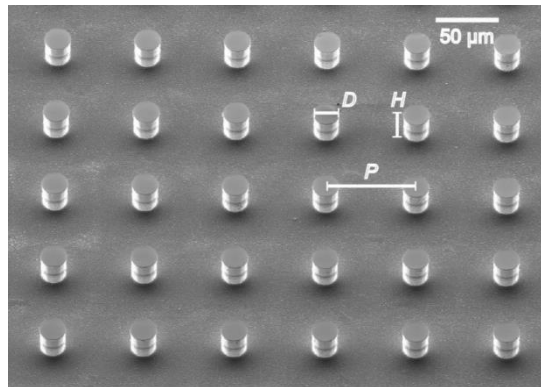
2. Experimental methodology
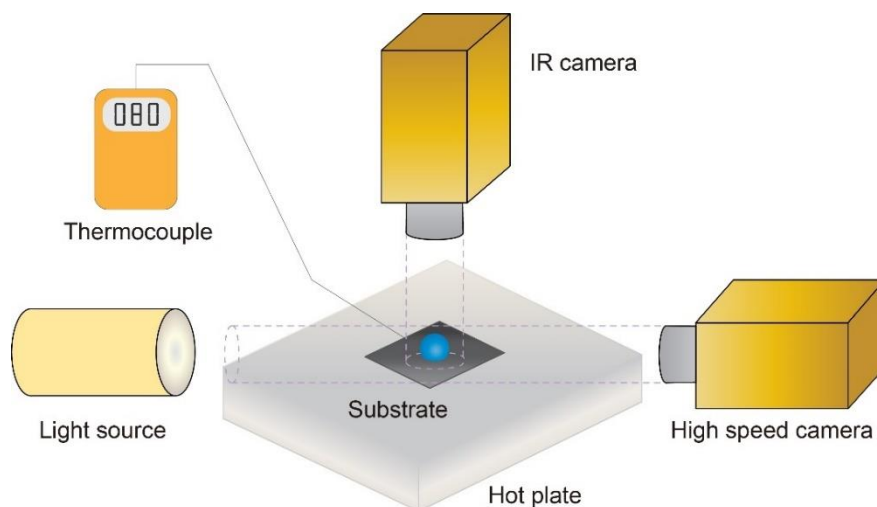
2.1 Substrates with micropillars

Micropillars patterned on a silicon wafer were manufactured by standard contact photolithography process and deep reactive ion etching method[5, 42-44]. Three kinds of substrates of 1 mm thick and textured with cylindrical micropillar arrays with varying micropillar periodicity (P) were used in this study. The geometry information of the substrates is listed in Table 1 and the scanning electron microscope (SEM) image of one sample substrate is shown in Fig. 1. All the substrates were conformally coated with silane (Trichloro (1H,1H,2H,2H-per fluorooctyl)-silane, Sigma-Aldrich) using standard chemical vapor deposition (CVD) process for superhydrophobicity enhancement[45]. Then the substrates were baked on a hot plate at 100 °C for 60 min. Water droplet exhibits a contact angle of $155° \pm 2°$ on all the as-prepared substrates. To mitigate the sample edge effect on the droplet evaporation process, substrate samples were cut into square pieces with the dimension of 2 cm × 2 cm and water droplets were deposited at the center of the substrate for evaporation study.

Table 1. Micropillar diameter, periodicity and height on the sample substrates

Substrate	Micropillar diameter D (µm)	Micropillar periodicity P (µm)	Micropillar height H (µm)
Sample 1	20	40	40
Sample 2	20	50	40
Sample 3	20	60	40

Figure 1. Scanning electron micrograph of the sample device with regularly patterned micropillars for droplet evaporation study.

Figure 2. Schematic diagram of the experimental setup including IR camera, substrate with micropillars, hot plate, light source, thermocouple and high-speed CCD camera mated to an optical tensiometer.

2.2 Experimental setup

The schematic of the experimental setup is shown in Fig. 2. In this study, deionized (DI) water (Type 1, >18 MΩ cm resistivity) was used as the liquid and a DI water droplet of 4 ± 0.1 μL generated by a syringe pump (EW-74905, Cole-Parmer Corporation) was gently dispensed on the center of the micro-structured substrate for evaporation study. At least five trials were carried out for each droplet evaporation experiment to ensure the repeatability of the evaporation measurements. Because of the small volume, the shape of the sessile water droplet resembled a spherical cap. The substrates were affixed on a hot plate by double-side copper tape and a K-type thermocouple with ±0.5 °C uncertainty was used to measure the surface temperature of the substrate during the experiment. The base temperature of the substrate was maintained at a constant level on the hot plate ranging from 40 °C to 120 °C, beyond which even a small temperature increase would otherwise lead to the onset of boiling of the sessile droplet. Two cameras parallel and normal to the substrate were used to record the evaporation process of the droplets. A calibrated infrared (IR) camera (FILR A5) was fixed above the droplet and normal to the substrate to measure the surface temperature evolution of the droplet. A water droplet sitting on the superhydrophobic substrate exhibits a large contact angle and only the upper hemispherical surface of the droplet can be focused by the IR camera. Regardless of the influence of droplet internal flow on its surface

6

temperature distribution, the temperature measured by the IR camera was taken as the average surface temperature of the upper hemispherical cap of the droplet. Aligned in parallel to the substrate, a high-speed CCD camera mated with an optical tensiometer (Theta Lite, OneAttension Corporation) was used to capture the images of the evaporating droplet. The droplet shape is assumed to be axisymmetric. Based on the captured snapshots, the water droplet was divided into multiple layers and the local height and diameter of each water layer were obtained by image processing. Then, the droplet volume was calculated by integrating the volume of each discrete layer. With the snapshots obtained by the high-speed camera, the transient droplet volume, contact angle, contact radius and droplet height were collected for subsequent analysis. During the experiment, the ambient temperature and relative humidity were maintained at $T_{\mathrm{lab}} = 23 \pm 2°C$ and $R_{\mathrm{h}} = 35 \pm 5\%$, respectively.

3. Experimental model

3.1 Wetting state

Water droplets can exhibit different wetting states on the micro-structured substrate during the evaporation. Specific air/vapor cavities underneath the droplet were observed during the majority time of the evaporation, which means the droplet was at least partially in the Cassie state. At the very end of the evaporation, water was observed to fill the cavities underneath the droplet and the droplet was in the Wenzel state during this period. The snapshots of the water droplet during evaporation are shown in the supplementary materials. Though the droplet exhibited two distinct wetting states during evaporation, the droplet stayed in the Cassie state during most of the evaporation process. In this work, we focus on the evaporation process of the droplet in the Cassie state and the thermal circuit model developed by us is based on the Cassie state droplet.

3.2 Energy balance model

When a droplet is deposited on the hot substrate, heat will transfer from the hot plate through the micro-micropillared substrate into the sessile droplet due to the temperature difference between the hot substate base and the droplet surface as shown in Fig. 3(a). This heat transfer process will result in the temperature increase inside the droplet and accelerate the heat and mass transfer

between the droplet and the ambient air. The energy balance of the evaporating sessile droplet is given by:

$$q_s = q_{\text{temp}} + q_{\text{conv}} + q_{\text{rad}} + q_{\text{evap}} \qquad (1)$$

where q_s is the overall heat transfer rate from the substrate to the droplet, q_{temp} is the energy transfer rate for the bulk water temperature increase, q_{conv} is the convective heat transfer rate between the water droplet and the ambient air, q_{rad} is the radiation heat transfer rate from the droplet surface to the ambient, and q_{evap} is the evaporation heat transfer rate. So, we have:

$$q_{\text{temp}} = c_w \rho_w V \frac{dT_{\text{cap}}}{dt} \qquad (2)$$

$$q_{\text{rad}} = \varepsilon \sigma S \left(T_{\text{cap}}^4 - T_\infty^4 \right) \qquad (3)$$

$$q_{\text{conv}} = h_{\text{conv}} S \left(T_{\text{cap}} - T_\infty \right) \qquad (4)$$

$$q_{\text{evap}} = h_{\text{fg}} \rho_w \frac{dV}{dt} \qquad (5)$$

where c_w, ρ_w, T_{cap}, V and h_{fg} are the specific heat capacity, density, droplet cap surface temperature, volume and latent heat of the water droplet, respectively; ε is the emissivity of the water droplet surface and σ is the Stefan-Boltzmann constant; S is the liquid-vapor interface area and h_{conv} is the natural convection heat transfer coefficient of the ambient air.
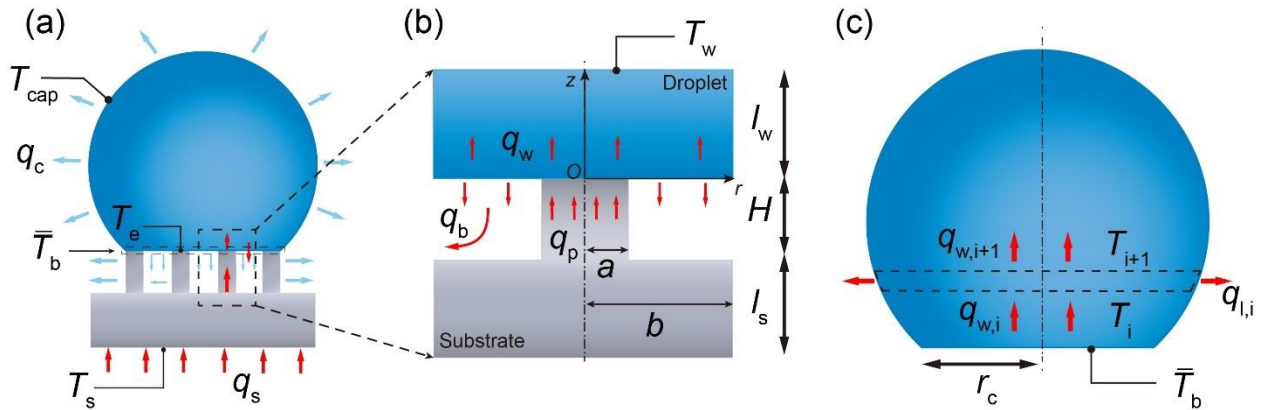
Figure 3. (a) Diagram of droplet evaporation on hot micro-structured superhydrophobic subface. (b) Diagram of heat transfer from a micropillar unit into droplet base surface. (c) Diagram of heat transfer inside the water droplet.

Because of the high efficiency of phase change heat transfer, the heat transfer rate induced by evaporation q_{evap} is dominant over the other heat transfer modes. Thus, the overall heat transfer from the substrate to the water droplet can be estimated as the heat released from the droplet to the ambient by evaporation[19]. Therefore, the energy balance equation can be rewritten as:

$$q_s = q_{\text{evap}} \tag{6}$$

3.3 Evaporation from droplet base surface

Droplet evaporation occurs at the liquid-vapor interface. For a Cassie state droplet on a micro-structured substrate, there exist air/vapor cavities between the droplet base and the substrate. Different from a sessile droplet on a smooth surface, with which the droplet base is in direct contact, only part of the droplet base is in touch with the surface roughness on a micro-structured substrate. The existence of the liquid-vapor interface at the droplet base leads to evaporation therein. In previous evaporation studies of the Cassie state droplet on micro-structured surfaces at room temperature, the evaporation from the droplet base was generally neglected and only the evaporation from the droplet cap was taken in to consideration[38]. It is reasonable to neglect the evaporation from the droplet base at room temperature considering the relatively small liquid-vapor interface area and the high relative humidity in the surface cavities. However, for a Cassie state droplet on a hot micro-structured substrate, the hot substrate will cause a direct temperature rise of the droplet base, making the evaporation from the droplet base nonnegligible. As shown in Fig. 3(a), both the evaporation from the droplet cap and the base surface should be taken into account for the thermal analysis of a Cassie state droplet on hot micro-structured surfaces.

Because of the periodicity of the micropillar arrays, the heat transfer process in one unit of micropillar cell can be representative of the heat transfer process between the droplet base and the substrate micropillars[18]. Thus, we focus on the heat transfer from one micropillar cell into the droplet base as illustrated in Fig. 3(b). A unit of the micropillar cell consists of one micropillar and the cavity around it. In general, heat transfer from both the silicon substrate and the vapor cavity should be considered. However, the thermal resistance of the vapor layer is much larger than the thermal resistance of the silicon micropillar due to the order of magnitude difference in the thermal

conductivities of silicon micropillars (100 W·m^{-1}·K^{-1})[18] and water vapor (0.025 W·m^{-1}·K^{-1})[39]. Therefore, it is reasonable to assume that heat primarily conducts from the micropillar to the water droplet while the vapor-solid interface of the cavity can be regarded as adiabatic.

As mentioned before, heat transferred from the substrate is equal to that released to the ambient. Thus, we can calculate the substrate heat transfer rate based on the decreasing rate of the droplet volume (Eq. 5). Thus, heat transfer rate in one unit cell could be calculated as:

$$q_{\text{p}} = \frac{q_{\text{s}}}{N} \tag{7}$$

where N is the total number of the micropillars underneath the droplet, *i.e.*, the ratio of the droplet apparent contact area to one unit cell area.

The thermal resistance per unit cell of the silicon substrate could be calculated as:

$$R_{\text{s}} = \frac{l_{\text{s}}}{k_{\text{Si}}P^2} + \frac{4H}{k_{\text{Si}}\pi D^2} \tag{8}$$

where k_{Si} is the thermal conductivity of silicon and l_{s} is the thickness of the silicon substrate excluding the height of the micropillar.

Based on the energy balance inside the silicon substrate, the temperature on the tip of the micropillar could be calculated as:

$$T_{\text{p}} = T_{\text{s}} - \frac{q_{\text{p}}}{R_{\text{s}}} \tag{9}$$

Considering the heat flux at the liquid-solid interface, the contact temperature at the liquid vapor interface is given by[16, 46-48]:

$$T_{\text{e}} = \frac{\sqrt{\rho_{\text{w}}k_{\text{w}}c_{\text{w}}}T_{\text{o}} + \sqrt{\rho_{\text{Si}}k_{\text{Si}}c_{\text{Si}}}T_{\text{p}}}{\sqrt{\rho_{\text{w}}k_{\text{w}}c_{\text{w}}} + \sqrt{\rho_{\text{Si}}k_{\text{Si}}c_{\text{Si}}}} \tag{10}$$

where ρ, c and k are the density, specific heat and thermal conductivity of water (w) and silicon (Si), respectively; T_{o} is the initial temperature of the water droplet.

To estimate the temperature distribution near the liquid-solid interface, *i.e.*, at the tip of the micropillar in contact with the droplet base, a thin water layer with a thickness of l_{w} in a unit cell (Fig. 3b) is considered. Assuming convection heat transfer is secondary in this water film[36], the conductive heat transfer equation therein is:

$$\frac{\partial^2 T}{\partial r^2} + \frac{1}{r}\frac{\partial T}{\partial r} + \frac{\partial^2 T}{\partial z^2} = 0 \tag{11}$$

Due to the relatively small size of the micropillar, the heat flux across the liquid-solid interface and the liquid-vapor interface in a unit cell could be assumed as uniform. As a result, we have the first boundary condition:

$$k_w \frac{\partial T}{\partial z} = \begin{cases} \dfrac{q_p}{\pi a^2} & 0 < r < a; \quad z = 0 \\[2ex] -\dfrac{q_b}{\pi(b^2 - a^2)} & a < r < b; \quad z = 0 \end{cases} \tag{12}$$

where k_w is the thermal conductivity of water, a is the radius of the micropillar, b is the radius of one unit cell[49], q_b is the heat transfer rate from the droplet base-vapor interface within one unit cell as shown in Fig. 3(b).

Temperature inside the water layer is assumed to become uniform soon. Hence, a uniform temperature boundary could be assumed at $z = l_w$:

$$T(r; z) = T_w \qquad 0 < r < b; \quad z = l_w \tag{13}$$

Moreover, considering the periodicity of the unit cells, we assume the adiabatic boundary between the chosen unit cell and its neighboring cells inside the water layer. Thus, we obtain the adiabatic boundary condition:

$$\frac{\partial T}{\partial r} = 0 \qquad r = b; \quad 0 < z < l_w \tag{14}$$

Solving the heat transfer equation Eq. (11) with the three boundary conditions Eqs. (12)-(14), we can obtain the temperature distribution inside the water layer as:

$$T_b(r,z) = T_w + \frac{q_p(l_w - z)}{\pi k_w}\left(\frac{(1-\varphi)}{b^2}\right) + \frac{2a q_p}{\pi k_w}\left(\frac{1}{a^2} + \frac{\varphi}{b^2 - a^2}\right)\sum_{n=1}^{\infty}\left[J_1\left(\frac{a}{b}\alpha_n\right)J_0\left(\frac{r}{b}\alpha_n\right)/\right.$$

$$\left.\left(\alpha_n^2 J_0^2(\alpha_n)\right)\right]\frac{\sinh\left(\frac{\alpha_n}{b}(l_w - z)\right)}{\cosh\left(\frac{\alpha_n}{b}l_w\right)} \tag{15}$$

where φ is the evaporation ratio, *i.e.*, the heat transfer across the droplet base-vapor interface over the overall heat transfer from the substrate to the droplet $\varphi = q_b/q_p$. Here $J_0(x)$ and $J_1(x)$ are the first kind Bessel functions with orders of 0 and 1, respectively, α_n is the nth root of $J_1(x) = 0$ [50].

The temperature at the droplet base ($z = 0$) is calculated as:

$$T_b(r,0) = T_w + \frac{q_p l_w}{\pi k_w}\left(\frac{(1-\varphi)}{b^2}\right) + \frac{2aq_p}{\pi k_w}\left(\frac{1}{a^2} + \frac{\varphi}{b^2-a^2}\right)\sum_{n=1}^{\infty}\left[J_1\left(\frac{a}{b}\alpha_n\right)J_0\left(\frac{r}{b}\alpha_n\right)/\right.$$

$$\left.\left(\alpha_n^2 J_0^2(\alpha_n)\right)\right]\tanh\left(\frac{\alpha_n}{b}l_w\right) \tag{16}$$

Thus, the average temperature of the droplet base could be obtained as:

$$\bar{T}_b = \frac{\int_0^b 2\pi r T_b(r)dr}{\pi b^2} \tag{17a}$$

$$\bar{T}_b = T_w + \frac{q_p l_w}{\pi k_w}\left(\frac{(1-\varphi)}{b^2}\right) \tag{17b}$$

The average temperature of the solid-liquid interface at the droplet base could be estimated as:

$$T_{b,p} = \frac{\int_0^a 2\pi r T_b(r)dr}{\pi a^2} \tag{18a}$$

$$T_{b,p} = \bar{T}_b + \left\{\frac{2aq_p}{\pi k_w}\left(\frac{1}{a^2} + \frac{\varphi}{b^2-a^2}\right)\sum_{n=1}^{\infty}\left[J_1^2\left(\frac{a}{b}\alpha_n\right)/\left(\alpha_n^3 J_0^2(\alpha_n)\right)\right]\tanh\left(\frac{\alpha_n}{b}l_w\right)\right\} \tag{18b}$$

The temperature at the solid-liquid interface should be same as the contact temperature, we have:

$$T_{b,p} = T_e \tag{19}$$

Thus, the average temperature of the water droplet base is given by:

$$\bar{T}_b = T_e - \frac{q_p 2a(1+k)}{k_w}\sum_{n=1}^{\infty}\left[J_1^2\left(\frac{a}{b}\alpha_n\right)/\left(\alpha_n^3 J_0^2(\alpha_n)\right)\right] \tag{20}$$

3.4 Evaporation from droplet cap surface

Regarding the evaporation of a sessile water droplet especially at a relatively low temperature, the one-dimensional heat conduction process inside the droplet is shown in Fig. 3(c). The water droplet is discretized into a series of thin layers ($i = 1, \dots X$, where X is the total number of water layers) parallel to the substrate. Here, temperatures at the bottom surface (T_i) and the top surface (T_{i+1}) of the ith water layer are assumed to be laterally uniform, respectively. Then, in the ith water layer, we have:

$$T_{i+1} = T_i - q_{w,i} \cdot R_i \tag{21}$$

where $R_i = \frac{\Delta h}{k_w \pi r_i^2}$ is the thermal resistance of the ith water layer, Δh is the thickness of each water layer, and r_i is the radius of the ith water layer.

Taking the ith layer as the control volume, heat transfer into the ith water layer from the bottom

surface ($q_{w,i}$) is balanced by the heat transfer to the top surface ($q_{w,i+1}$) and the evaporation rate ($q_{l,i}$) from the side surface. Thus, the energy balance in the ith water layer is:

$$q_{w,i+1} = q_{w,i} - q_{l,i} \tag{22}$$

where $q_{l,i} = J_i(r) \cdot h_{fg} \cdot \Delta S_i$, ΔS_i is the side surface area of the ith water layer, h_{fg} is the latent heat, and $J_i(r)$ is the local evaporation mass flux.

Then we applied the diffusion-driven model to estimate the local evaporation flux, which is the solution to the Laplace equation based on Fick's law of vapor diffusion around the droplet. Hence, the exact solution of the local evaporation flux is given by[31]:

$$J(r) = \frac{D_d\left(c_s(T_i) - R_h c_s(T_\infty)\right)}{r_c} \cdot \left[\frac{1}{2}\sin(\theta) + \sqrt{2}\left(\cosh(\beta) + \cos(\theta)\right)^{3/2} \cdot \right.$$
$$\left. \int_0^\infty \frac{\cosh(\theta\tau)}{\cosh(\pi\tau)} \tan[(\pi - \theta)\tau] \cdot P_{-0.5+i\tau}\left(\cosh(\beta)\right)\tau \cdot d\tau \right] \tag{23}$$

where T_i is approximated to be the temperature at the side surface, c_s is the saturated vapor concentration, D_d is the diffusion coefficient of vapor, and R_h is the relative humidity. And β is the toroidal coordinate related uniquely to the cylindrical coordinate r on the cap surface.

The evaporation heat transfer rate from the droplet cap surface is calculated by integrating all the local evaporation rates:

$$q_c = \sum_{i=1}^{X} q_{l,i} \tag{24}$$

The evaporation heat transfer from the droplet cap should be the same as the heat transferred through the water droplet:

$$q_c = (1 - \varphi)q_s \tag{25}$$

As mentioned above, the temperature measured by the IR camera can be taken as the average temperature of the upper hemispherical surface. With the average droplet base temperature obtained, we can calculate the surface temperature distribution based on the heat transfer equation Eq. (21) for the discretized water layers. Thus, we can approximate the average temperature of the upper hemispherical surface of the droplet as:

$$T_{model} = \sum_{i=1}^{M} T_i \cdot \Delta S_i / 2\pi r_w^2 \tag{26}$$

where M is the number of discrete water layer in the upper hemisphere of the droplet spherical cap,

r_w is the radius of the spherical cap.

3.5. Algorithm for calculating the surface temperature and evaporation ratio

The algorithm for calculating the droplet surface temperature and the evaporation ratio φ is shown in the flowchart of Fig. 4. The base temperature of the substrate T_s is measured by the thermocouple and the heat transfer rate from the substrate q_s is obtained by calculating the droplet volume decreasing rate based on Eq. (5). An initial estimate of the evaporation ratio $\varphi = 0.5$ is used in the boundary condition to solve the heat transfer equation Eq. (11) at the droplet base. Then the temperature distribution at the droplet base is calculated by Eq. (16) and consequently the average temperature of the droplet base $\bar{T}_b$ is obtained. The nonuniform surface temperature distribution of the droplet cap is calculated based on the one-dimensional heat conduction model inside the droplet and the evaporation rate q_c from the droplet cap is then obtained. The evaporation heat transfer from the droplet cap should be the same as the heat transfer through the droplet body from the droplet base and the value of φ' is then obtained by Eq. (25) as the new evaporation ratio in the next step iteration calculating. After the iteration loop achieves convergence, both the stable evaporation ratio φ and temperature distribution on the droplet cap surface are obtained. With the droplet cap surface temperature distribution obtained, the average temperature of the upper hemispherical surface of the droplet cap surface T_{model} is calculated and compared with the experimental results for the validation of our thermal circuit model.

It is not practical to directly calculate the evaporation rate from the droplet base because of the complex micro-pillared structures in this study. Thus, the evaporation rate from the droplet base is taken as the difference of the total evaporation rate and the evaporation rate from the droplet cap. The predicting of droplet cap surface evaporation rate is based on the diffusion-driven model with the consideration of droplet surface temperature distribution (Eqs. 23 and 24). The validation of the evaporation rate prediction can be confirmed by Gleason and Putnam's report[51]. They predicted the droplet evaporation rate with diffusion-driven model with the consideration of droplet surface temperature distribution and the evaporation rate errors of this method were 1.84% and 2.83% for droplet evaporation on a substrate at 50 °C and 65 °C, respectively.
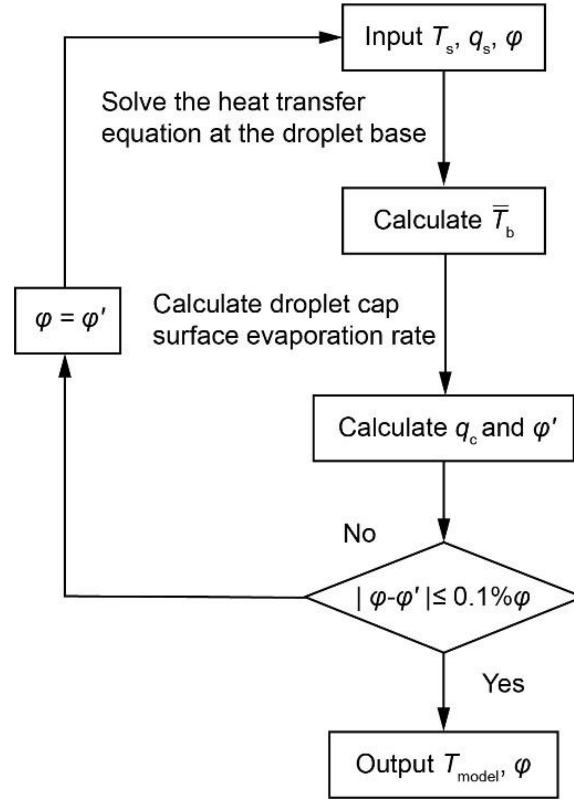
Figure 4. Flowchart for calculating the droplet surface temperature and evaporation ratio φ, which is defined as the ratio of evaporation rate from the droplet base surface to the total heat transfer rate.

## 4. Result and discussion

4.1. Droplet evaporation dynamics

The temporal evolutions of the droplet volume on different substrates are shown in Fig. 5. Droplet volume decreases nonlinearly during the evaporation. The total evaporation time decreases with the rise of the substrate base temperature. At the same substrate base temperature, the total evaporation time increases with the increasing micropillar periodicity. It can be seen in Fig. 5 that at each substrate base temperature, droplet evaporation on sample 3 (60 μm periodicity) has the longest total evaporation time and on sample 1 (40 μm periodicity) has the shortest total evaporation time. This increase of total evaporation time is ascribed to the increase of the thermal resistance between the droplet base and the substrate, which is caused by the increase of the micropillar periodicity. The total evaporation time of droplet evaporation on different sample substrates with varying base temperatures is shown in Table 2.

15
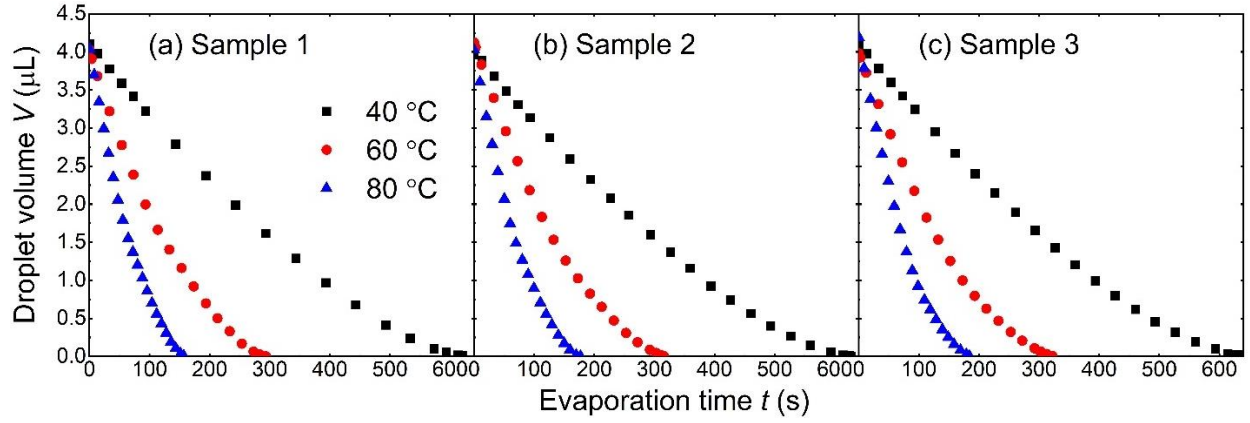
Figure 5. Temporal evolution of droplet volume on (a) sample 1, (b) sample 2 and (c) sample 3. The substrate of each sample was heated to 40 °C, 60 °C and 80 °C, respectively.

Table 2. Total evaporation time for water droplet of 4 µL on micro-pillared substrates with different base temperatures.

Substrate	Substrate base temperature (°C)	Total evaporation time (s)
Sample 1	40	620.1
	60	293.3
	80	156.8
Sample 2	40	627.1
	60	312.2
	80	177.1
Sample 3	40	633.3
	60	322.3
	80	184.1
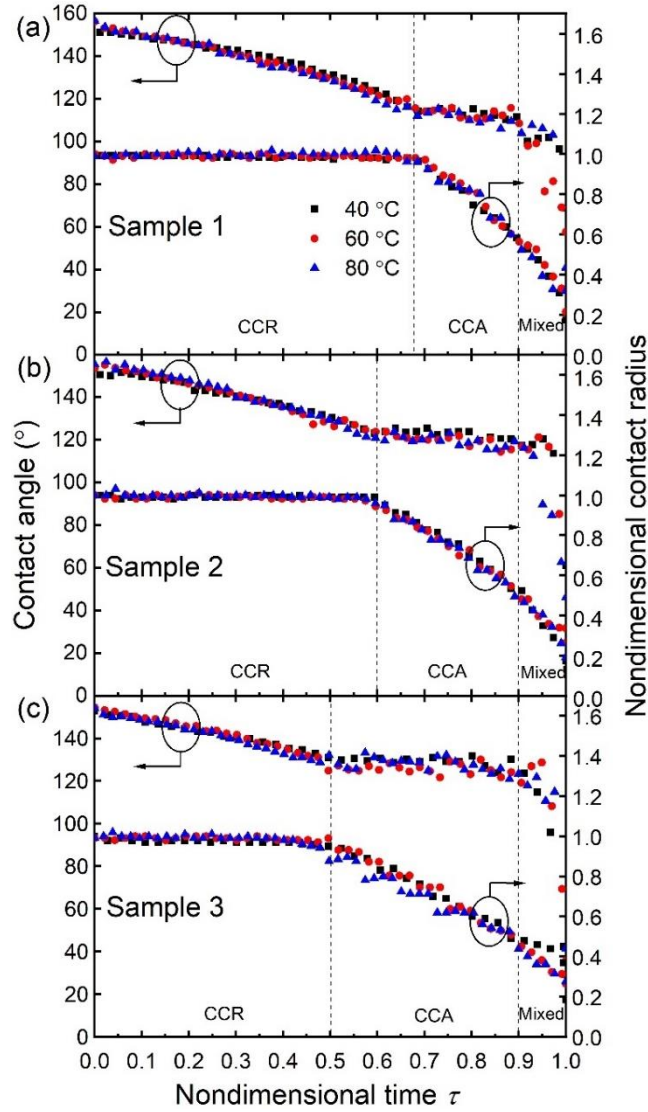
Figure 6. Evolution of droplet contact angle and nondimensional contact radius versus nondimensional time on (a) sample 1, (b) sample 2 and (c) sample 3. Each substrate base was heated to 40 °C, 60 °C and 80 °C, respectively.

The evolutions of droplet contact angle and nondimensional contact radius with nondimensional time are shown in Fig. 6. Here the nondimensional contact radius is defined as the ratio of the contact radius to the initial contact radius, and the nondimensional time is defined as the ratio of the evaporation time to the total evaporation time. It can be seen from Fig. 6 that the evolutions of droplet contact angle and nondimensional contact radius are almost the same for droplet evaporation on each sample substrate with different base temperatures. For droplet evaporation on sample 1 (Fig. 6a), the droplet contact angle continuously decreased during the

first 68% portion of the total evaporation time while the contact radius was unchanged, which is the constant contact radius (CCR) mode for droplet evaporation. After the contact angle reached the receding contact angle, the contact angle stopped decreasing and was maintained at a constant level while the contact radius started to decrease, which is the constant contact angle (CCA) mode for droplet evaporation. The droplet evaporation was kept in the CCA mode till the nondimensional time approached 0.9. Then, both the contact angle and contact radius started decreasing, which is the mixed mode for droplet evaporation. For droplet evaporation on the same sample with different substrate temperatures, the evaporation process had almost the same compositions of the CCR, CCA and mixed modes, indicating that the substrate structure is more influential on the evaporation mode transition than the substrate temperature at least within a certain range (*i.e.*, ≤ 80 °C). The evolutions of droplet contact angle and nondimensional contact radius on sample 2 (Fig. 6b) and sample 3 (Fig. 6c) are similar to the evaporation on sample 1. It is noteworthy that the receding contact angle increases with the increasing periodicity of micropillars on the substrates. The receding contact angles on sample 1, sample 2 and sample 3 are about 112°, 120° and 128°, respectively. Since the initial contact angles of water droplets on these three samples are almost the same (about 155°), a larger receding contact angle results in the shorter term of the CCR mode. The nondimensional evaporation times for the CCR mode on sample 1, sample 2 and sample 3 are about 0.68, 0.6 and 0.5, respectively.

4.2. Experimental and modelled droplet cap surface temperature

The evolutions of droplet cap temperature versus the nondimensional time on samples 1, 2 and 3 are shown in Figs. 7(a), (b) and (c), respectively. For droplet evaporation on substrates with temperature in the range of 40 °C – 80 °C, the droplet cap temperature predicted by the thermal circuit model matches well with that measured by the IR camera. There exists a large temperature gradient between the droplet cap surface and the substrate base, which is caused by the thermal resistances of the water droplet, the evaporation at the droplet surface and the conduction through the silicon substrate. It can be seen in Fig. 7 that average temperature of droplet cap increased in the CCR mode and kept almost constant in the CCA mode. Similar trends were also observed by

Saenz et al.[52] in their numerical simulation of droplet evaporation on heated surfaces. During the CCR mode, the thermal resistance of the droplet decreases with the decreasing droplet volume. Meanwhile, the droplet cap gets closer to the substrate and thus the droplet cap temperature increases. During the CCA mode, the contact area between the droplet base and the substrate continuously decreases. As a result, less heat is transferred into the droplet, hindering the temperature increase of the droplet. During the CCA mode, the shrinking contact area between the droplet base and the substrate results in the almost unchanged temperature on the droplet cap. In the mixed mode, the volume of the evaporating droplet is relatively small (< 0.05 µL) and droplet evaporation in this mode is not a focus in this discussion.
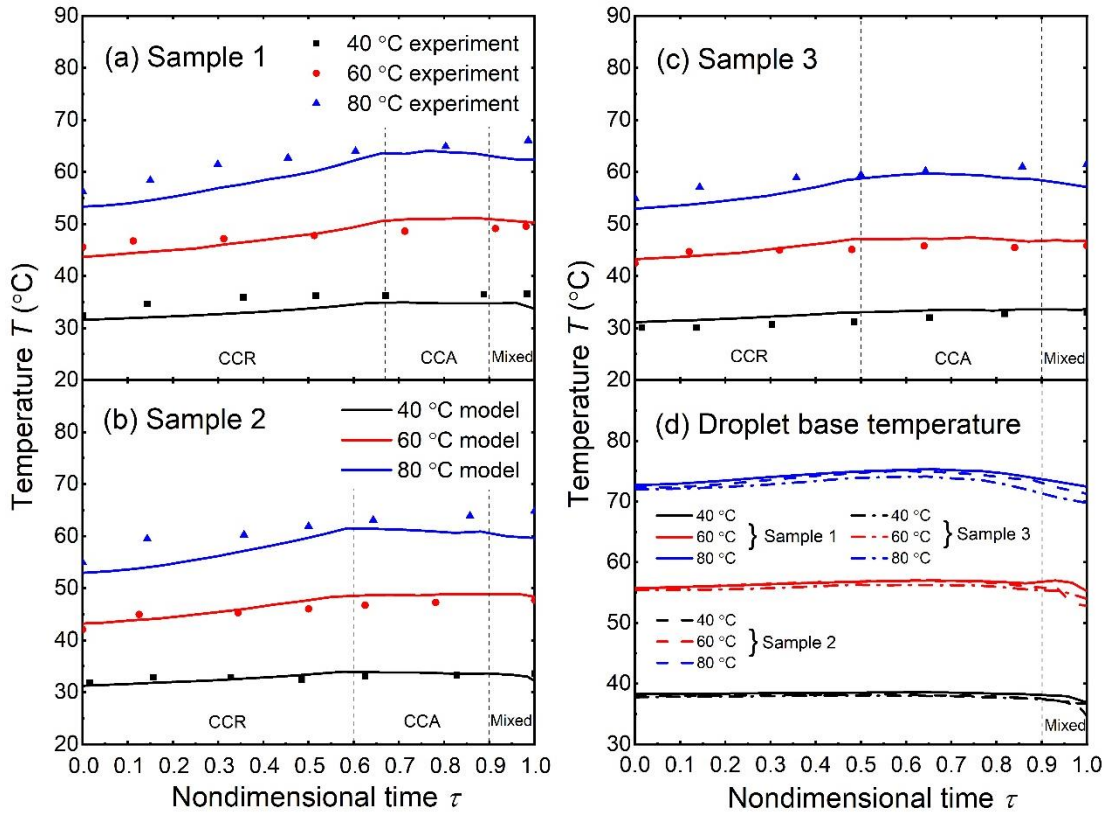
Figure 7. Evolution of droplet cap surface temperature on (a) sample 1, (b) sample 2, and (c) sample 3. The solid lines represent the droplet cap surface temperature calculated by the thermal circuit model and the scatter dots are the experimental results obtained by the IR camera. (d) Evolution of droplet base temperature on sample 1, sample 2 and sample 3 with the substrate temperature heated at 40 °C, 60 °C and 80 °C, respectively.

The average temperature of the droplet base on different samples and with different substrate

temperatures is shown in Fig. 7(d). There exists an apparent temperature mismatch between the droplet base and the substrate base. Though there is a temperature drop through the substrate because of the substrate's conduction resistance, the large thermal conductivity of silicon (300 W/m·K) should have led to a very small thermal resistance. As such, the temperature drop through the substrate is < 1°C based on our calculated results. However, the temperature mismatches between the droplet base and the substrate base are about 2 °C, 5 °C and 8 °C on substrates with the base temperature at 40 °C, 60 °C and 80 °C, respectively. It is plausible that such an apparent temperature difference between the droplet base and the substrate base may be mainly caused by the evaporation from the droplet base in substrate cavities.
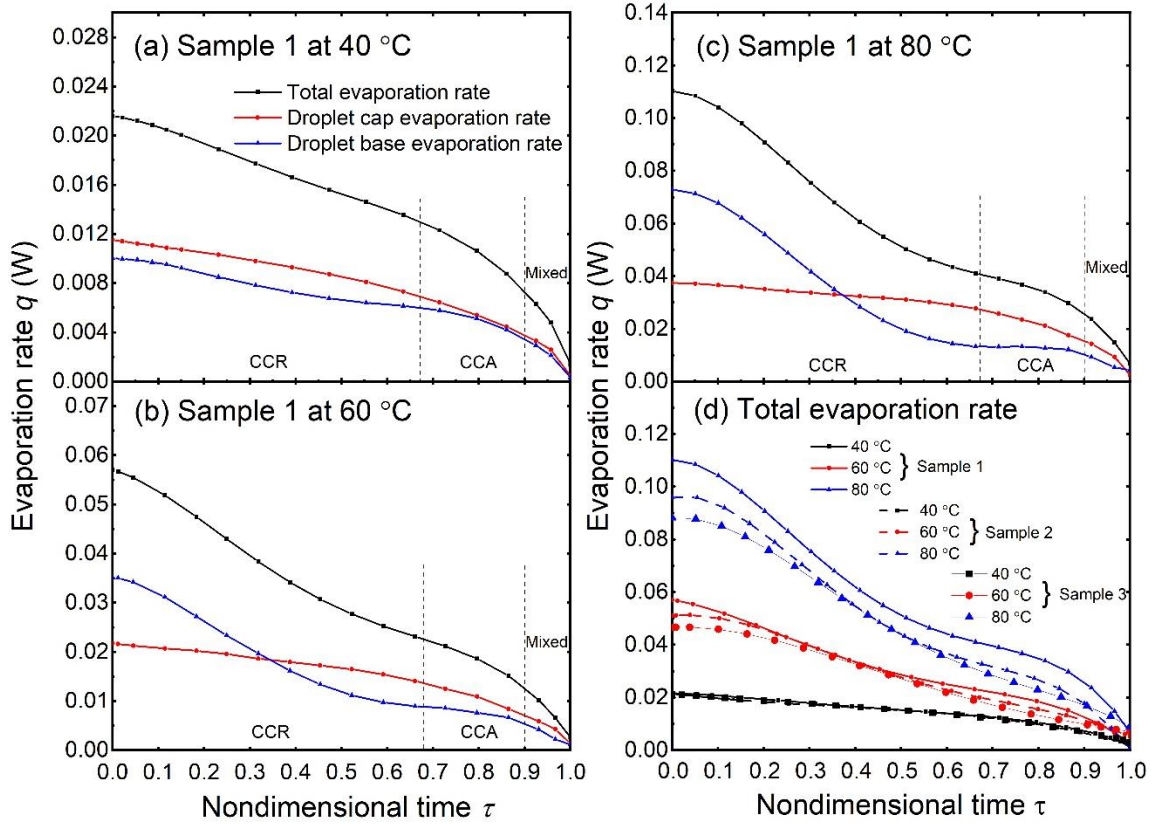
Figure 8. Total evaporation rate, droplet cap surface evaporation rate and droplet base evaporation rate on sample 1 with (a) 40 °C substrate base temperature, (b) 60 °C substrate base temperature and (c) 80 °C substrate base temperature. (d) Total evaporation rate on samples 1, 2 and 3 with substrate base temperature at 40 °C, 60 °C and 80 °C, respectively.

In Figs. 8(a), (b) and (c), we show the transient evolutions of the total evaporation rate, the evaporation rate from droplet cap and the evaporation rate from droplet base on sample 1 with the

substrate base temperature maintained at 40 °C, 60 °C and 80 °C, respectively. The corresponding evaporation rates of water droplets on sample 2 and sample 3 are given in the supplementary materials. The total evaporation rate of water droplet is calculated by Eq. (5) and (6), *i.e.*, the droplet volume decreasing rate. The evaporation rate from the droplet cap surface is calculated by the diffusion-driven model with the cap surface temperature distribution predicted by the thermal circuit model. The evaporation rate from the droplet base is the difference between the total evaporation rate and the droplet cap surface evaporation rate. Obviously, the increase of the substrate temperature would lead to the evaporation enhancement from both the droplet cap surface and the droplet base surface. Also, both the evaporation rates from the droplet cap and from the droplet base decrease during droplet evaporation on a substrate with a constant temperature. It can be observed that in the CCR mode the slope of the evaporation rate from the droplet cap is smaller than that at the droplet base, which means a lower decreasing speed of the evaporation rate from the droplet cap. In the CCR mode, the reduction of the droplet contact angle will result in the decrease of the droplet cap surface evaporation rate. Meanwhile, the temperature increase of the droplet cap surface will improve the local evaporation rate. The effect of droplet cap temperature increase compensates the depressed effect of the droplet contact angle decrease on the evaporation from the droplet cap. The combined effects of the contact angle decrease and the droplet cap temperature increase give rise to the slow decrease of the evaporation rate from the droplet cap in the CCR mode. In the CCA mode, the average temperature of the droplet cap keeps essentially constant, which is in contrary to the increasing trend of the droplet cap temperature in the CCR mode. Meanwhile, the contact radius of the droplet decreases in the CCA mode, which causes the decreasing heat transfer area between the droplet and the substrate. Thus, the evaporation rate from the droplet cap decreases quickly in the CCA mode. In summary, in the CCR mode the decrease of the total evaporation rate of the droplet is mainly caused by the decreasing evaporation rate from the droplet base. Whereas in the CCA mode, the decrease of the total evaporation rate is mainly induced by the decreasing evaporation rate from the droplet cap.

Droplet evaporation on different substates exhibits distinct evaporation rates as shown in Fig.

8(d). Droplet on sample 1 (40 μm periodicity) has the maximum evaporation rate while droplet has the minimum evaporation rate on sample 3 (60 μm periodicity). Due to the different periodicities of micropillars, the droplet-pillar interface areas are different on these sample substrates. Since water droplets on these sample substrates have almost the same apparent contact area (*i.e.*, base area of the droplet), small periodicity of micropillars means larger heat transfer area between the droplet base and the substrate, *i.e.*, the solid-liquid interface area. The larger solid-liquid interface area results in the higher droplet evaporation rate with the same substrate base temperature.
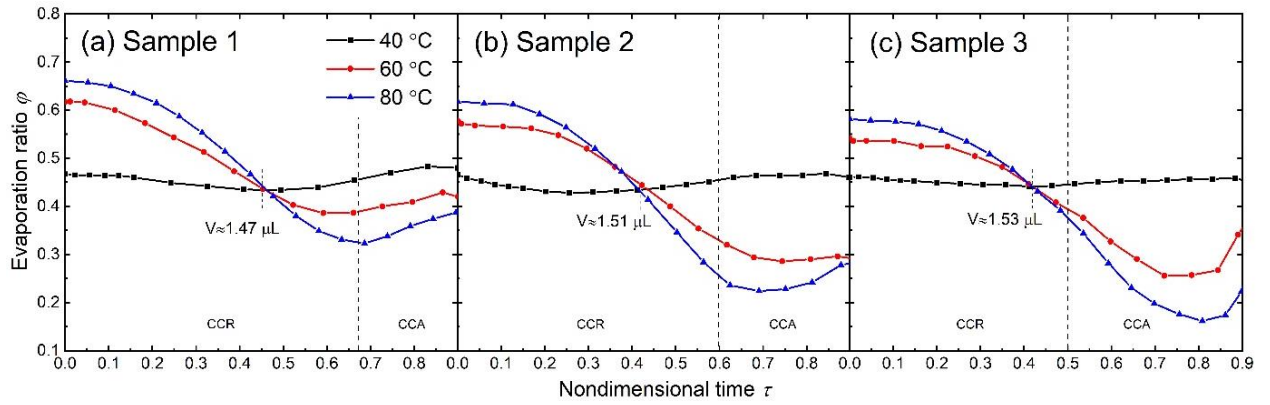
Figure 9. Evaporation ratio φ of water droplets with respect to nondimensional time on different micro-structured samples with different substrate base temperatures.

Evaporation ratio φ is defined as the ratio of the evaporation rate from the droplet base to the total evaporation rate. The evaporation ratio φ with respect to nondimensional time on different samples with different substrate base temperatures is shown in Fig. 9. It can be observed that the evaporation ratio φ generally decreases in the CCR mode while increasing close to the end of the CCA mode. This phenomenon is mainly caused by the larger decreasing rate of evaporation from the droplet base in the CCR mode and the relatively smaller decreasing rate of evaporation in the CCA mode, compared with the evaporation rate from the droplet cap. Generally, the evaporation ratio φ increases with the substrate temperature for droplet evaporation on the same substrate with a relatively large volume. The increase of the substrate temperature will directly cause a temperature increase at the droplet base and subsequently induce the temperature increase at the droplet cap. Due to the thermal resistance of the droplet bulk, the temperature increase at the

droplet cap is smaller than that at the droplet base in response to the substrate temperature increase. Thus, more evaporation occurs from the droplet base than from the droplet cap with the increase of the substrate temperature. It is observed from Fig. (9) that the evaporation ratio φ decreases with the increase of the substrate temperature after the droplet volume shrinking to less than about 1.5 μL. This opposite variation of the evaporation ratio is caused by the decrease of droplet volume. When the droplet volume shrinks to about the 1.5 μL, both the droplet height and the droplet cap surface area decrease rapidly, *e.g.*, the surface area of the droplet cap is reduced by half. As a result, the thermal resistance of the droplet bulk is comparatively small, and the increase of the substrate temperature will cause a higher temperature rise at the droplet cap. Thus, stronger evaporation occurs from the droplet cap than from the droplet base with the increase of the substrate temperature and therefore the evaporation ratio decreases.

4.3. Effective conductivity of water droplet for evaporation on high temperature substrate

We further conducted droplet evaporation experiments on the same micro-structured surfaces with even higher temperatures. Figs. 10(a), (b) and (c) show the evolutions of droplet cap temperature during droplet evaporation on different samples with the substrate temperature at 100 °C and 120 °C, respectively. The dash lines are the droplet cap temperatures calculated by the thermal circuit model. For droplet evaporation on a substrate with a relatively low temperature (40 °C – 80 °C), the droplet cap temperature calculated by the thermal circuit model matches well with the experimental results. However, for droplet evaporation on a high temperature substrate, there exist large deviations between the model-predicted results and the experimental measurements. These derivations are due to the internal fluid flow of the droplet, which is not taken into account in the thermal circuit model. The effects of droplet internal flow are not significant for droplet evaporation on relatively low temperature substates (40 °C – 80 °C). As mentioned by Dash and Garimella[36], the characteristic velocity of fluid flow in a 3 μL water droplet evaporating on a 40 °C – 60 °C substrate is of tens of microns per second and the Peclet number is less than 1. Thus, it is reasonable for us to only consider the conduction heat transfer while neglecting the internal convection of the water droplet on a substrate with a relatively low

temperature (40 °C – 80 °C). With the further increase of substrate temperature, more heat is transferred through the droplet and the temperature difference between the droplet top and bottom becomes larger. Fluid motion driven by the temperature gradient in the droplet becomes violent and the characteristic velocity of internal flow increases. Thus, we need to account for the effects of the droplet internal flow in the thermal circuit model for high temperature evaporation analysis.

Driven by the surface tension gradient (caused by the surface temperature gradient), water at the droplet bottom will flow upwards, which will in turn minish the temperature gradient on the droplet surface. As a result, the upper hemispherical part of the droplet will get warmed up by the up flowing hot water, and the temperature of the upper hemispherical portion should become higher than the case without internal flow considered. To account for the effect of internal fluid flow, the overall averaged cap surface temperature is calculated as the modified temperature:

$$T'_{\text{model}} = \sum_{i=1}^{X} T_i \cdot \Delta S_i / 2\pi r_w^2 (1 - \cos\theta) \tag{27}$$
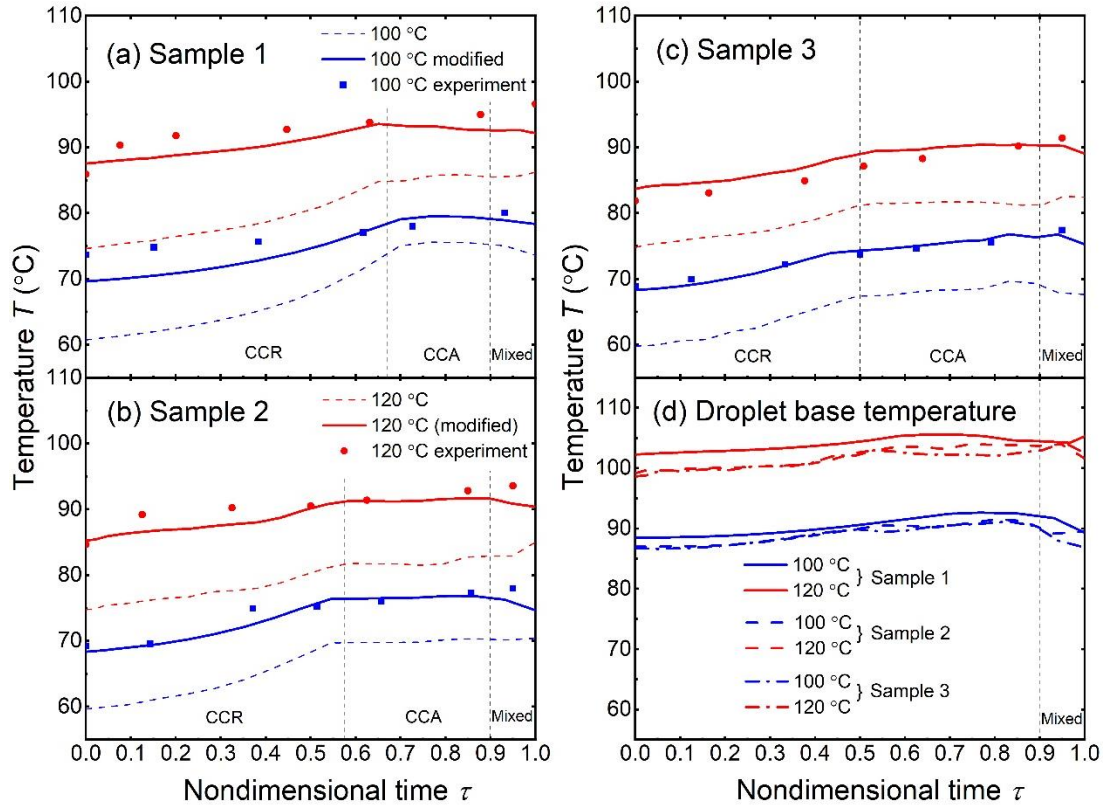
Figure 10. Evolution of droplet cap temperature on (a) sample 1, (b) sample 2 and (c) sample 3. The dash lines represent the droplet cap temperatures calculated by thermal circuit model, the solid lines represent the droplet cap temperatures modified with total average temperature and effective

24

conductivity, and the scatter dots are the experimental results by IR camera. (d) Evolution of droplet base temperature on samples 1, 2 and 3 with substrate temperature at 100 °C and 120°C, respectively.

As shown in Figs. 10(a), (b) and (c), the modified temperature calculated by Eq. (27) matches well with the experimental data for droplet evaporation on samples 1, 2 and 3 with the substrate base temperature maintained at 100 °C.

But there still exist large derivations between the modified results and the experimental data for droplet evaporation on samples with the substrate temperature heated up to 120 °C. In this scenario, the convection heat transfer in the droplet cannot be neglected. In the thermal circuit model, only the conductive thermal resistance of the droplet is taken into account. Convection inside the droplet will remarkably enhance heat transfer therein and reduce the total thermal resistances of the droplet. Because of the complexity of internal flow, it is not practical to analyze the convection heat transfer simply based on the droplet characteristic velocity. Alternatively, an effective thermal conductivity is adopted to account for both the convection and conduction heat transfer in the droplet. As such, the effective conductivity[53] of an evaporating droplet is defined as:

$$k_{\mathrm{eff,w}} = e \cdot k_w \tag{28}$$

where e is a coefficient of the effective conductivity.

The effective conductivity $k_{\mathrm{eff,w}}$ is adopted in the thermal circuit model in place of the original water conductivity k_w to account for both the conduction and the convection heat transfer in the droplet. The effect of convection in the heat transfer is equivalent as an increase of the thermal conductivity of the working fluid. The minimum value of e allowing for the average difference between the model predicted surface temperature and the experimental value less than 2 °C, *i.e.*, $\left| \bar{T}_{\mathrm{model}} - \bar{T}_{\mathrm{expt}} \right| \leq 2\ °C$, is chosen as the coefficient of the effective conductivity.

The coefficient e for the effective thermal conductivity of droplet evaporation on samples 1, 2 and 3 with substrate temperature of 120 °C is found to be 3.2, 2.9 and 2.7, respectively. Our results of coefficient e are very close to the numerical fitting coefficient 2.72 obtained by Abramzon and Sirignano[53]. Actually, these substrates had been heated to a level over the boiling temperature

of water droplet. However, no boiling was observed in the droplet even with the substrate temperature reaching 120 °C, which is possibly due to the evaporative cooling at the droplet base. As evaporation at the droplet base will cool down the local surface temperature, we calculated the average temperature of the droplet base as shown in Fig. 10(d). For droplet evaporation on the 100 °C substrate, the base temperature was about 88 °C and for droplet evaporation on the 120 °C substrate, the base temperature was about 102 °C, which is very close to the saturation temperature of 100 °C. Our analysis show that evaporation cooling from the droplet base can significantly delay the onset of droplet boiling with the substrate temperature even reaching 120 °C.

5. Conclusions

In this work, the evaporation of water droplet on hot micro-structured superhydrophobic surfaces has been experimentally and theoretically investigated. Prior studies about the effects of substrate temperature on the sessile droplet evaporation mainly focused on the Leidenfrost effect[39, 54, 55], in which the droplet is levitated by the evaporating vapor on a very high temperature substrate (200 °C – 300 °C). Only a few studies investigated the sessile droplet evaporation dynamics on substrates with a relative low temperature (40 °C – 100 °C) and very limited attention had been paid to the evaporation from the droplet base that becomes amplified with the increasing substrate temperature. Here, for the first time, we conducted a comprehensive thermal resistance analysis for the sessile droplet evaporation on hot micro-structured superhydrophobic substrates to analyze the evaporation from both the droplet cap and the droplet base. According to our theoretical analysis, droplet cap temperature shows distinct trends in different evaporation modes, *i.e.*, droplet cap temperature increases in the CCR mode while keeping almost constant in the CCA mode. The total evaporation rate of the droplet decreases during the evaporation process. In the CCR mode, the decrease of the total evaporation rate of the droplet is mainly caused by the decreasing evaporation rate from the droplet base. And in the CCA mode, the decrease of the total evaporation rate is mainly induced by the decreasing evaporation rate from the droplet cap. The evaporation ratio φ decreases in the CCR mode and increases approaching the end of the CCA mode. Meanwhile, the evaporation ratio φ increases with the

increase of the substrate temperature when droplet volume is relatively large during the evaporation. Then after the droplet shrinking to a small volume, the evaporation ratio φ decreases with the increase of the substrate temperature. Internal fluid motion affects the droplet evaporation process on substrates with a high temperature (100 °C – 120 °C) and an effective thermal conductivity $k_{\text{eff,w}}$, which is about three times of water conductivity k_w, is employed by us as a correction factor for the thermal circuit model to account for the convection heat transfer in the water droplet. Furthermore, the average temperature at the droplet base is calculated and a large temperature difference between the droplet base and the substrate surface is observed. The apparent temperature differences between the droplet base and the substrate base are about 2 °C, 5 °C, 8 °C, 12.5 °C and 18 °C for the evaporating droplet on the micro-structured substrates with the base temperature maintained at 40 °C, 60 °C, 80 °C, 100 °C and 120 °C, respectively. Our study about the sessile droplet evaporation on hot micro-structured superhydrophobic surfaces can deepen our understanding of the heat and mass transfer not only from the droplet cap but also from the droplet base. Moreover, this thermal circuit model provides us a convenient tool to analyze the evaporation dynamics of a sessile droplet on hot micro-structured substrates.

6. CRediT authorship contribution statement

[†]**Wenge Huang** and **Xukun He** are co-first authors with equal contribution to this work. **Wenge Huang:** Conceptualization, Methodology, Investigation, Formal analysis, Writing – Original Draft. **Xukun He:** Conceptualization, Methodology, Writing – Review & Editing. **Jiangtao Cheng:** Conceptualization, Writing – Review & Editing, Supervision, Project administration, Funding acquisition. **Cong Liu:** Resources. **Xiaojie Li:** Resources. **Yahua Liu:** Resources, Supervision, Funding acquisition.

7. Declaration of Competing Interest

None.

8. Acknowledgment

Nomenclature

a	radius of micropillar [μm]
b	radius of water/substrate layer in one unit cell [μm]
c_{Si}	specific heat capacity of silicon [J/(kg·K)]
c_s	saturated vapor concentration [kg/m^3]
c_w	specific heat capacity of water [J/(kg·K)]
D	diameter of micropillar [μm]
D_d	coefficient of vapor diffusion [m^2/s]
e	coefficient of effective conductivity
H	height of micropillar [μm]
h_{conv}	convection heat transfer coefficient of air [W/(m^2·K)]
h_{fg}	latent heat of water [kJ/kg]
J	local evaporation flux [kg/(m^2·s)]
$k_{eff,w}$	effective conductivity of water [W/(m·K)]
k_{Si}	thermal conductivity of silicon [W/(m·K)]
k_w	thermal conductivity of water [W/(m·K)]
l_s	thickness of silicon substrate [μm]
l_w	thickness of water layer [μm]
M	number of water layer in the upper hemisphere of the droplet spherical cap
N	number of micropillars under the droplet base
n	order of Bessel function
P	periodicity of substrate [μm]
q_b	heat transfer rate from droplet base in one unit cell [W]
q_{conv}	convective heat transfer rate [W]
q_c	evaporation heat transfer rate from droplet cap surface [W]
q_{evap}	evaporation heat transfer rate of water droplet [W]
q_l	heat transfer rate from the side surface water layer [W]
q_p	heat transfer rate in one unit cell [W]
q_{rad}	radiative heat transfer rate [W]
q_s	heat transfer rate from droplet base [W]
q_{temp}	heat transfer rate for droplet temperature increase [W]
q_w	heat transfer rate in the water layer in one unit cell [W]
R_h	relative humidity
R_i	thermal resistance of water layer [K/W]
R_s	thermal resistance of substrate [K/W]
r	radius of water droplet [μm]
r_w	radius of spherical cap droplet [μm]
S	surface of spherical cap [μm^2]
$\bar{T}_b$	average temperature of droplet base [K]

$T_{b,p}$	average temperature of solid-liquid interface [K]	
T_{cap}	temperature of droplet cap surface [K]	
T_e	contact temperature at the solid-liquid interface [K]	
T_{expt}	droplet surface temperature tested by the IR camera	
T_i	temperature of control volume water layer [K]	
T_{lab}	lab ambient temperature [K]	
T_{model}	average temperature calculated by the thermal circuit model [K]	
T_o	initial temperature of droplet base [K]	
T_p	top surface temperature of micropillar [K]	
T_w	uniform temperature of water layer in one unit cell [K]	
T_∞	ambient temperature [K]	
V	volume of water droplet	
X	total number of water layer	
Greek symbols		
α	root of Bessel function	
ε	emissivity of water	
θ	contact angle of water droplet [°]	
ρ	density [kg/m^3]	
σ	Stefan-Boltzmann constant [kg/(s^3·K^4)]	
τ	nondimensional evaporation time	
φ	evaporation ratio	
Abbreviations		
CCA	constant contact angle	
CCR	constant contact radius	
DI	deionized	
IR	infrared	
SEM	scanning electron microscope	

9. Reference

[1]. P. Calvert, Inkjet Printing for Materials and Devices, Chem. Mater., 13 (10) (2001) 3299-3305.

[2]. Y. Jiang, C. Wu, L. Li, K. Wang, Z. Tao, F. Gao, W. Cheng, J. Cheng, X.-Y. Zhao, S. Priya, and W. Deng, All electrospray printed perovskite solar cells, Nano Energy, 53 (2018) 440-448.

[3]. A. Wu, L. Yu, Z. Li, H. Yang, and E. Wang, Atomic force microscope investigation of large-circle DNA molecules, Anal Biochem, 325 (2) (2004) 293-300.

[4]. W. Jia and H.H. Qiu, Experimental investigation of droplet dynamics and heat transfer in spray cooling, Exp. Therm. Fluid Sci., 27 (7) (2003) 829-838.

[5]. J. Song, W. Cheng, M. Nie, X. He, W. Nam, J. Cheng, and W. Zhou, Partial Leidenfrost Evaporation-Assisted Ultrasensitive Surface-Enhanced Raman Spectroscopy in a Janus Water Droplet on Hierarchical Plasmonic Micro-/Nanostructures, ACS Nano, 14 (8) (2020) 9521-9531.

[6]. X. He and J. Cheng, Evaporation-triggered directional transport of asymmetrically confined droplets, Journal of Colloid and Interface Science, 604 (2021) 550-561.

[7]. S.A. Putnam, A.M. Briones, L.W. Byrd, J.S. Ervin, M.S. Hanchak, A. White, and J.G. Jones, Microdroplet evaporation on superheated surfaces, International Journal of Heat and Mass Transfer, 55 (21) (2012) 5793-5807.

[8]. P. Tsai, R.G. Lammertink, M. Wessling, and D. Lohse, Evaporation-triggered wetting transition for water droplets upon hydrophobic microstructures, Physical review letters, 104 (11) (2010) 116102.

[9]. L. Zhao and J. Cheng. Contact Line Dynamics of Water Droplets Spreading on Nano-Structured Teflon Surfaces in Dropwise Condensation. in Heat Transfer Summer Conference. 2017. American Society of Mechanical Engineers.

[10]. L. Zhao and J. Cheng, The mechanism and universal scaling law of the contact line friction for the Cassie-state droplets on nanostructured ultrahydrophobic surfaces, Nanoscale, 10 (14) (2018) 6426-6436.

[11]. X. He, L. Zhao, and J. Cheng, Coalescence-Induced Swift Jumping of Nanodroplets on Curved Surfaces, Langmuir, 35 (30) (2019) 9979-9987.

[12]. L.S. Lam, M. Hodes, and R. Enright, Analysis of Galinstan-Based Microgap Cooling Enhancement Using Structured Surfaces, Journal of Heat Transfer, 137 (9) (2015)

[13]. A. Al-Sharafi, B.S. Yilbas, and H. Ali, Droplet Heat Transfer on Micropost Arrays With Hydrophobic and Hydrophilic Characteristics, Journal of Heat Transfer, 140 (7) (2018)

[14]. C.-C. Hsu, Y.-A. Lee, C.-H. Wu, and C.S.S. Kumar, Self-propelled sessile droplets on a superheated and heterogeneous wetting surface, Colloids and Surfaces A: Physicochemical and Engineering Aspects, 612 (2021)

[15]. F.G.H. Schofield, S.K. Wilson, D. Pritchard, and K. Sefiane, The lifetimes of evaporating sessile droplets are significantly extended by strong thermal effects, Journal of Fluid Mechanics, 851 (2018) 231-244.

[16]. B. Sobac and D. Brutin, Thermal effects of the substrate on water droplet evaporation, Phys Rev E 86 (2 Pt 1) (2012) 021602.

[17]. K. Gleason, H. Voota, and S.A. Putnam, Steady-state droplet evaporation: Contact angle influence on the evaporation efficiency, International Journal of Heat and Mass Transfer, 101 (2016) 418-426.

[18]. S. Adera, R. Raj, R. Enright, and E.N. Wang, Non-wetting droplets on hot superhydrophilic surfaces, Nat. Commun., 4 (2013) 2518.

[19]. R. Hays, D. Maynes, and J. Crockett, Thermal transport to droplets on heated superhydrophobic substrates, Int. J. Heat Mass Transfer, 98 (2016) 70-80.

[20]. M.S. Hanchak, A.M. Briones, J.S. Ervin, and L.W. Byrd, One-dimensional models of nanoliter droplet evaporation from a hot surface in the transition regime, International Journal of Heat and Mass Transfer, 57 (2) (2013) 473-483.

[21]. S.Y. Misyura, Contact angle and droplet heat transfer during evaporation on structured and smooth surfaces of heated wall, Applied Surface Science, 414 (2017) 188-196.

[22]. M.A. Kadhim, N. Kapur, J.L. Summers, and H. Thompson, Experimental and Theoretical

Investigation of Droplet Evaporation on Heated Hydrophilic and Hydrophobic Surfaces, Langmuir, 35 (19) (2019) 6256-6266.

[23]. L. Liu, X. Liang, X. Wang, S. Kong, K. Zhang, and M. Mi, Evaporation of a sessile water droplet during depressurization, International Journal of Thermal Sciences, 159 (2021) 106587.

[24]. L. Bansal, S. Chakraborty, and S. Basu, Confinement-induced alterations in the evaporation dynamics of sessile droplets, Soft Matter, 13 (5) (2017) 969-977.

[25]. S. Semenov, F. Carle, M. Medale, and D. Brutin, Boundary conditions for a one-sided numerical model of evaporative instabilities in sessile drops of ethanol on heated substrates, Phys Rev E, 96 (6-1) (2017) 063113.

[26]. R.G. Picknett and R. Bexon, The evaporation of sessile or pendant drops in still air, Journal of Colloid and Interface Science, 61 (2) (1977) 336-350.

[27]. M.E.R. Shanahan, Simple Theory of "Stick-Slip" Wetting Hysteresis, Langmuir, 11 (3) (1995) 1041-1043.

[28]. N.N. Lebedev, Special Functions and Their Applications. Prentice-Hall. Englewood Cliffs, NJ, USA. 1965.

[29]. R.G.L. Hua Hu, Evaporation of a Sessile droplet on a substrate, J Phys Chem B, 106 (2002) 1334-1344.

[30]. Robert D. Deegan, Olgica Bakajin, Todd F. Dupont, Greg Huber, Sidney R. Nagel, and T.A. Witten, Contact line deposits in an evaporating drop, Phys Rev E, 62 (2000)

[31]. Y.O. Popov, Evaporative deposition patterns: spatial dimensions of the deposit, Phys. Rev. E 71 (3) (2005) 1-17.

[32]. T.A.H. Nguyen, A.V. Nguyen, M.A. Hampton, Z.P. Xu, L. Huang, and V. Rudolph, Theoretical and experimental analysis of droplet evaporation on solid surfaces, Chemical Engineering Science, 69 (1) (2012) 522-529.

[33]. H. Gelderblom, Á.G. Marín, H. Nair, A. van Houselt, L. Lefferts, J.H. Snoeijer, and D. Lohse, How water droplets evaporate on a superhydrophobic substrate, Physical Review E, 83 (2) (2011) 026306.

[34]. S. Dash and S.V. Garimella, Droplet evaporation dynamics on a superhydrophobic surface with negligible hysteresis, Langmuir, 29 (34) (2013) 10785-95.

[35]. A. Aldhaleai, F. Khan, T. Thundat, and P.A. Tsai, Evaporation dynamics of water droplets on superhydrophobic nanograss surfaces, International Journal of Heat and Mass Transfer, 160 (2020)

[36]. S. Dash and S.V. Garimella, Droplet evaporation on heated hydrophobic and superhydrophobic surfaces, Phys Rev E, 89 (2014) 042402.

[37]. R.N. Wenzel, Resistance of Solid Surfaces to Wetting by Water, Industrial & Engineering Chemistry, 28 (8) (1936) 988-994.

[38]. G. McHale, S. Aqil, N.J. Shirtcliffe, M.I. Newton, and H.Y. Erbil, Analysis of droplet evaporation on a superhydrophobic surface, Langmuir, 21 (2005) 11053-11060.

[39]. M. Wei, Y. Song, Y. Zhu, D.J. Preston, C.S. Tan, and E.N. Wang, Heat transfer suppression by suspended droplets on microstructured surfaces, Applied Physics Letters, 116 (23) (2020)

[40]. H.-m. Kwon, J.C. Bird, and K.K. Varanasi, Increasing Leidenfrost point using micro-nano hierarchical surface structures, Applied Physics Letters, 103 (20) (2013)

[41]. D. Tam, V. von Arnim, G.H. McKinley, and A.E. Hosoi, Marangoni convection in droplets on superhydrophobic surfaces, Journal of Fluid Mechanics, 624 (2009) 101-123.

[42]. J. Cheng, A. Vandadi, and C.-L. Chen, Condensation heat transfer on two-tier superhydrophobic surfaces, Appl. Phys. Lett., 101 (13) (2012)

[43]. A. Vandadi, L. Zhao, and J. Cheng, Resistant energy analysis of self-pulling process during dropwise condensation on superhydrophobic surfaces, Nanoscale Adv., 1 (3) (2019) 1136-1147.

[44]. X. Liu, P.R. Coxon, M. Peters, B. Hoex, J.M. Cole, and D.J. Fray, Black silicon: fabrication methods, properties and solar energy applications, Energy & Environmental Science, 7 (10) (2014) 3223-3263.

[45]. M. Badv, I.H. Jaffer, J.I. Weitz, and T.F. Didar, An omniphobic lubricant-infused coating produced by chemical vapor deposition of hydrophobic organosilanes attenuates clotting on catheter surfaces, Sci. Rep., 7 (1) (2017) 11639.

[46]. M. di Marzo and D.D. Evans, Evaporation of a water droplet deposited on a hot high thermal conductivity solid surface, (PB--86-247871/XAB) (1986) 34.

[47]. K.M. Itaru Michiyoshe, Heat transfer characteristics of evaporation of a liquid droplet on heated surfaces, international Journal of Heat and Mass Transfer, 21 (1977) 605-613.

[48]. M. Seki, H. Kawamura, and K. Sanokawa, Transient temperature profile of a hot wall due to an impinging liquid droplet, Journal of Heat Transfer, 100 (1987) 167-169.

[49]. Seri Lee, Seaho Song, Van Au, and K.P. Moran. Constriction Spreading resistance model for electroics packing. in ASME/JSME Thermal Engineering Conference. 1995.

[50]. D.P. Kennedy, Spreading Resistance in Cylindrical Semiconductor Devices, Journal of Applied Physics, 31 (8) (1960) 1490-1497.

[51]. K. Gleason and S.A. Putnam, Microdroplet evaporation with a forced pinned contact line, Langmuir, 30 (34) (2014) 10548-55.

[52]. P.J. Sáenz, K. Sefiane, J. Kim, O.K. Matar, and P. Valluri, Evaporation of sessile drops: a three-dimensional approach, Journal of Fluid Mechanics, 772 (2015) 705-739.

[53]. W.A.S. B. Abrambon, Droplet vaporization model for spray combusition calculations, International Journal of Heat and Mass Transfer, 32 (1989) 1605-1618.

[54]. D.A. del Cerro, A.G. Marin, G.R. Romer, B. Pathiraj, D. Lohse, and A.J. Huis in 't Veld, Leidenfrost point reduction on micropatterned metallic surfaces, Langmuir, 28 (42) (2012) 15106-10.

[55]. S.H. Kim, H. Seon Ahn, J. Kim, M. Kaviany, and M. Hwan Kim, Dynamics of water droplet on a heated nanotubes surface, Applied Physics Letters, 102 (23) (2013)

Click here to access/download
Supplementary Material
Supplementary Materials.pdf